© Strojniški vestnik 47(2001)8,441-448
ISSN 0039-2480
UDK 536.2
Izvirni znanstveni članek (1.01)

© Journal of Mechanical Engineering 47(2001)8,441-448
ISSN 0039-2480
UDC 536.2
Original scientific paper (1.01)

BYPASS EFFECT IN HIGH PERFORMANCE HEAT SINKS

Suzana Prstic, Madhusudan Iyengar, and Avram Bar-Cohen
Laboratory of the Thermal Management of Electronics
Department of Mechanical Engineering
University of Minnesota, Minneapolis, MN 55455
USA

ABSTRACT

Studies using commercial computational fluid dynamics software, running on a supercomputer, were carried out to investigate the effects of fin density, inlet duct velocity, and clearance area ratio, on the extent of flow bypass and its impact on the thermal performance of the heat sink. Flow bypass was found to increase with increasing fin density and clearance, while remaining relatively insensitive to inlet duct velocity. An optimum geometry, for a fixed inlet duct velocity, bypass clearance, fixed heat sink volume, and constant thickness, was determined.

INTRODUCTION

Continuing Moore's Law improvements in semiconductor technology are leading to larger, more complex integrated circuits with power dissipations and heat fluxes anticipated to reach 170W and 30W/cm2, respectively, by the middle of the current decade. Despite its relatively poor thermal properties, air continues to be the coolant of choice for many high-end electronic applications, necessitating the development of high-performance heat sinks, composed of thin, closely-spaced fins. The performance of such heat sinks is adversely affected by flow "by-pass," resulting from planned or inadvertent clearance gaps around the heat sink.

Early investigations of flow bypass phenomenon in longitudinal plate fin heat sink configurations include Sparrow et al [1978] and Sparrow and Kadle [1986], who studied the effect of tip clearance on thermal performance. These studies showed the ratio of heat transfer coefficients, with and without clearance, to be strongly influenced by the tip clearance to fin height ratio, and to be independent of air flow rate and fin height. Experimental results in Butterbaugh and Kang [1995] indicated the thermal resistance to correlate exclusively with the pressure drop in the duct across the heat sink, while appearing to be relatively independent of the amount of bypass. Analytical network flow based models using laminar flow in parallel plate channels have been presented in studies by Butterbaugh and Kang [1995], Lee [1995], and more recently by Reis and Altemani [1999]. Wirtz et al [1994] used analytical solutions for the heat transfer coefficient for developing flow between parallel plates, in conjunction with experimentally obtained data, to construct correlations for the prediction of heat sink thermal performance. This study also showed the existence of an optimum array design, for a given inlet flow condition and shroud configuration.

The experimental data collected for the various studies presented in literature, utilized heat sinks with relatively thick fins (≥ 1.27 mm) and moderate fin spacing (≥ 2.4 mm). The studies did not elaborate on the loss of airflow from the top of the heat sink ("leakage"), and the distribution of airflow through the various regions of the duct. The objective of the current work is to examine these phenomena in detail, using numerical CFD modeling.

The present paper begins with a discussion of the analytical heat transfer and fluid mechanics relations that govern the behavior of compact heat sinks and the geometries needed to achieve the desired cooling capability. Next, the laboratory apparatus used to experimentally characterize these compact heat sinks will be described, along with the results of experiments with fully- and partially-shrouded compact heat sinks. For validation purposes a comparison of these results, with values obtained using analytical and numerical (CFD) techniques, have been presented. Attention is then turned to the use of commercial computational fluid dynamics

(CFD) software to explore the effect of bypass on the thermal capability of three candidate heat sink designs, over a range of clearance area ratios and air mass flow rates. The thermal resistances and distribution pattern of these three heat sink designs are compared. To demonstrate the existence of an optimum geometry for a fixed inlet duct velocity and bypass clearance, the array geometry was optimized for a fixed heat sink volume, by varying the fin spacing while using fins of constant thickness.

ANALYTICAL MODELING OF SHROUDED HEAT SINKS

The analytical model developed by Holahan et al in [1996] for calculating the thermal and pressure drop performance in fully shrouded, laminar, parallel plate heat sinks has been utilized to characterize the thermofluid performance of parallel plate heat sinks. The model represents the flow field as a Hele Shaw flow and fin conduction is characterized using the superposition of a kernel function determined from the method of images. A 2-D flow field was assumed in the parallel plate channel between adjacent fins with uniform heating in the heat sink base and was shown to give good agreement with the 1-D results of Iwasaki et al [1994]. The side-inlet-side-exit (SISE) configuration considered in the current study is depicted in Figure 1, showing the nomenclature of the array geometry, including the fin height, H, fin thickness, t, inter-fin spacing, s, width of base, W, and the length of the heat sink base, L.

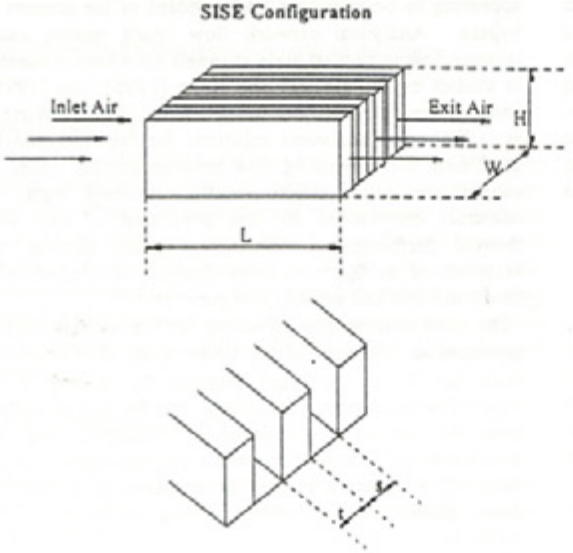

Figure 1. Side-Inlet-Side-Exit (SISE) Rectangular Plate Fin Heat Sink Configuration

Holahan et al [1996] discretized the plate fin into a number of patches, and the local heat transfer coefficient was determined from the straight duct flow correlation for developing thermal and hydrodynamic laminar flow in parallel plates with uniform wall temperature, provided in Kakac et al [1987] and given by,

$$h_{x,isoT} = \frac{k_{air}}{2s}\left[7.55 + \frac{(0.024X^{-1.14})\,0.0179Pr^{0.17}X^{-0.64} - 0.14}{(1+0.0358Pr^{0.17}X^{-0.64})^2}\right] \quad (1)$$

where, k_{air} is the air thermal conductivity, and $Pr = \nu/\alpha$ is the Prandtl number with ν as the mean kinematic viscosity of air and α the thermal diffusivity. In eq. (1), X is the dimensionless axial distance, and is given by,

$$X = \frac{[x\,\nu]}{4s^2 U_m Pr} \quad (2)$$

where x is the distance along the stream tube from the fin entrance to the patch, and U_m is the mean air velocity. The heat transfer from a patch is determined using the temperature difference for each patch, which is calculated using the superposition of a kernel function determined from the method of images. The heat dissipation from the heat sink array, q, is then found by the summation of patch heat transfer.

Three aluminum heat sinks occupying a volume 110 × 71 × 51 mm, as illustrated in Figure 4(b), with fin thickness of 0.5 mm were studied. The performance was determined analytically for volumetric airflow rates between 0.005 and 0.04 m^3/s (10.594 – 84.756 cfm). The thermal performance was characterized using the thermal resistance, R_{hs}, defined as

$$R_{hs} = \frac{\theta_b}{q} \quad (K/W) \quad (3)$$

where θ_b is the excess temperature of the heat sink base (K), and q is the total heat sink heat dissipation (W). The overall pressure drop developed by Holahan et al [1996] across the heat sink is based on correlations for laminar duct flow and is estimated by dividing the fin flow field into flowtubes. The total pressure model function including all the frictional and dynamic losses is defined as

$$\Delta P = \Delta P_{fd} + \frac{1}{2}\rho v_{in}^2 K(\infty) + \frac{1}{2}\rho v_{in}^2 K_c + \frac{1}{2}\rho v_{out}^2 K_e \quad (4)$$

where ΔP_{fd} is the frictional loss (Kakac et al 1987); K_c and K_e are contraction and expansion coefficients, respectively (Kays and London 1984); a term $K(\infty)$ is for hydrodynamic developing flat duct flow due to Chen (Kakac et al 1987) and v_{in} and v_{out} are inlet and outlet velocities, respectively. The thermal resistances and pressure drop for the three candidate heat sinks, as a function of volumetric flow rate and fin density are shown in Table 1 and Figure 2. From the Table 1 is observed that pressure drop across the heat sink increases with the inlet velocity as well as with the fin density.

Observing Figure 2, the thermal resistance is seen to improve with increasing fin density. However this heat transfer enhancement is accompanied by a significant pressure drop penalty as seen in Table 1. Considering the entire range of volumetric flow rates between 0.005 m^3/s and 0.04 m^3/s for the sparse, moderate and dense heat sinks, decreases in R_{hs} of 43%, 48% and 57 %, respectively, are accompanied by corresponding increases in ΔP by factors of 25, 17, and 14, respectively.

Table 1, Thermal Resistance and Pressure Drop for Three Candidate Heat Sinks

		Sparse Heat Sink N_{fin} = 16, s = 4.21mm		Moderate Heat Sink N_{fin} = 24, s = 2.57 mm		Dense Heat Sink N_{fin} = 32, s = 1.78 mm	
Vol. flow rate (m^3/s)	Velocity (m/s)	R_{hs}, K/W	ΔP, Pa	R_{hs}, K/W	ΔP, Pa	R_{hs}, K/W	ΔP, Pa
0.005	1.5	0.391	3.986	0.257	9.052	0.214	18.359
0.01	3	0.318	10.373	0.192	21.117	0.142	40.515
0.015	4.5	0.286	19.162	0.169	36.196	0.12	66.471
0.02	6	0.265	30.353	0.157	54.289	0.109	96.224
0.025	7.5	0.25	43.945	0.148	75.395	0.102	129.776
0.03	9	0.238	59.939	0.142	99.515	0.098	167.127
0.035	10.5	0.229	78.334	0.137	126.648	0.094	208.275
0.04	12	0.221	99.132	0.133	156.795	0.091	253.223

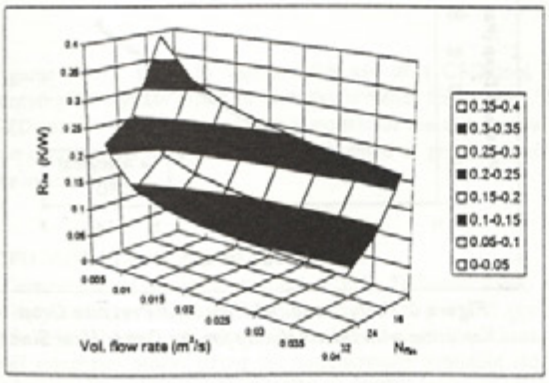

Figure 2, Thermal Resistance

The fully shrouded configuration is rarely encountered in real world applications, which typically include at least a small clearance around the heat sink. Under such circumstances, dense fin arrays might not prove to be the best design, due to flow bypass, which may be expected to diminish their thermal performance. This bypass effect will be numerically investigated in subsequent sections of this paper. Prior to this, experimental validation of the analytical and numerical models is presented.

EXPERIMENTAL INVESTIGATIONS

Experimental Setup

A wind tunnel was used to characterize the thermal performance and validate the analytical and CFD models of high performance heat sinks. A schematic of this experimental setup is depicted in Figure 3, showing its important components, i.e. the test section, the power supplies, the flow measurement devices, and the fan. The wind tunnel was designed to obtain a uniform velocity profile in the test section for inlet velocities ranging form 1m/s to 10 m/s.

The test section dimensions of 0.305 × 0.610 m allow a variety of heat sink sizes to be examined. Figure 4 shows the heat sink assembly mounted on a fiberglass-epoxy laminate board (FR-4), which serves to mimic supporting the chip package in an actual electronic system. The primary heater which is the power source to the heat sink, is located below the heater and on the top side of the fiber glass board. A PRT (Platinum Resistance Thermometers) which measures the temperature of the primary heater is located directly under it. The guard heater, used to eliminate heat loss from the bottom of the test section, and a PRT measuring its temperature, are located under the fiber glass board. RTD (Resistance temperature detector) devices are used to compare the temperatures of the two PRTs and provide the necessary information to the guard heater power supply controller, via a unit called the DTS (Differential Temperature Sensor).

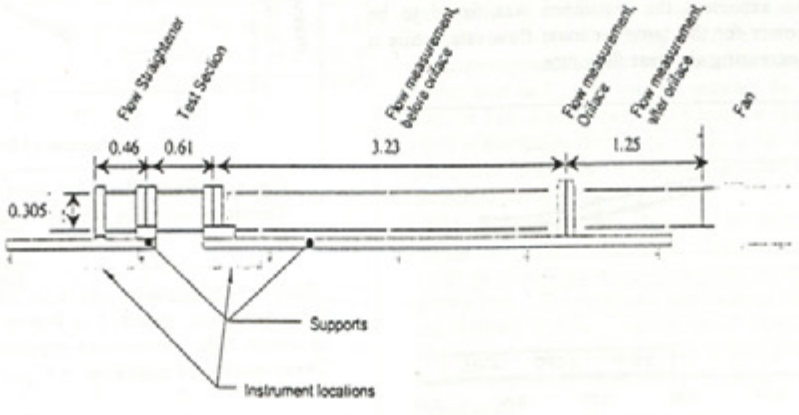

Figure 3, Wind Tunnel Set

Nine T-type thermocouples, 0.5 mm thickness, were attached to the base of the heat sink, in eight 10 mm drilled holes in the heat sink base and 1 mm slot in the center of the heat sink. The thermocouples are covered with silicone grease to improve the thermal contact with the heat sink base. Four thermocouples were also inserted at 40 mm upstream of the heat sink, and six at 30 mm downstream of the heat sink, to measure the inlet and outlet temperature air, respectively. All thermocouple and pressure sensors are connected to the data acquisition system and processed by Lab View software (National Instruments, 1998).

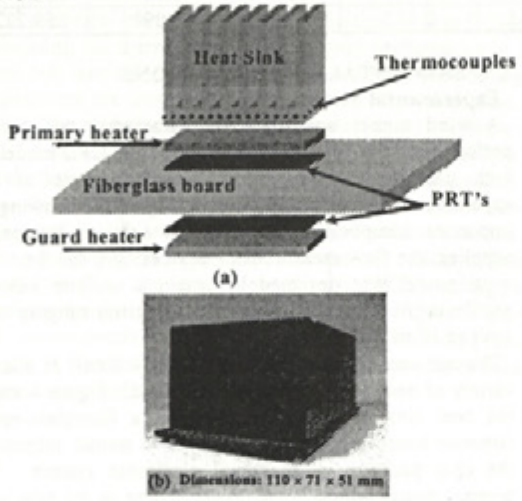

Figure 4, (a) Heat Sink Assembly, (b) Typical Heat Sink

Validation of CFD model

The thermal performance of a sample high performance heat sink shown, in Figure 4(b), was determined by experimental as well as numerical and analytical means, for several configurations to help evaluate its thermal capability. Figure 5 shows the thermal resistance, R_{over} that was determined experimentally using 100W heat input for a mass flow rate of 0.0174 kg/s (V_{inlet} = 3 m/s), 0.0247 kg/s (V_{inlet} = 4 m/s), 0.0297 kg/s (V_{inlet} = 5 m/s), and 0.0433kg/s (V_{inlet} = 7 m/s). In addition test runs for power inputs of 50W, 70W, and 120W were also carried out. As expected, the resistance was found to be invariant with power for the same air mass flow rate, while it decreased with increasing air mass flow rate.

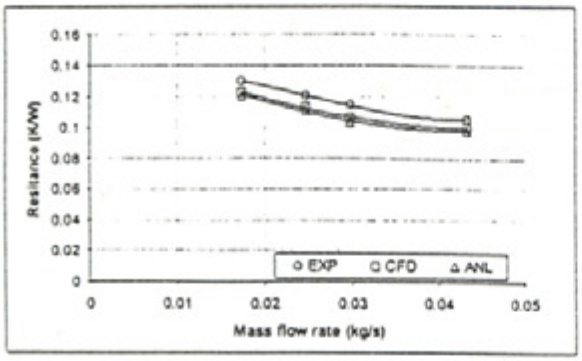

Figure 5, Fully Shrouded Heat Sink Resistance Variation with Flow Rate

As may be seen from Figure 5, all three modeling techniques displayed an identical trend and experimental data agreed to within 6 % with the CFD results and within 9 % with the analytical calculations.

The comparison between analytical and CFD pressure drop data for the dense heat sink is shown in Figure 6. The pressure drop is seen to increase parabolically with the inlet velocity and the analytical predictions are found to be within 8% of the CFD results.

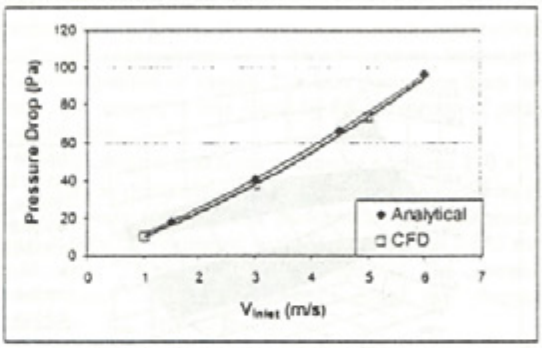

Figure 6, Fully Shrouded Heat Sink Pressure Drop Variation with Inlet Velocity for the Dense Heat Sink

Analytical and CFD results showing the variation of pressure drop with fin number are illustrated in Figure 7, for an inlet velocity of 3 m/s. Excellent agreement of 1 % was observed for the moderate heat sink while a larger discrepancy of 8% was found to occur for the dense heat sink.

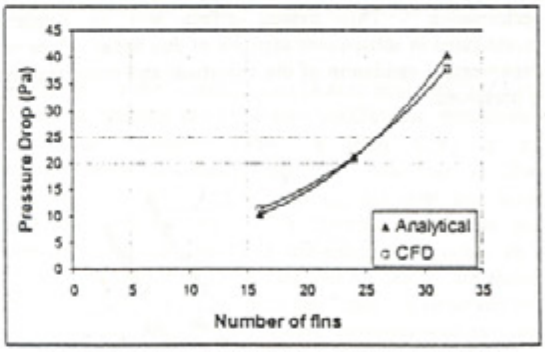

Figure 7, Fully Shrouded Heat Sink Pressure Drop Variation with Fin Density for 3 m/s Inlet Velocity

Such a comparison was also carried for the partially shrouded cases, depicted in Figure 10, yielding agreement to within 10% between the experimental and CFD results. These results are displayed in Figure 8.

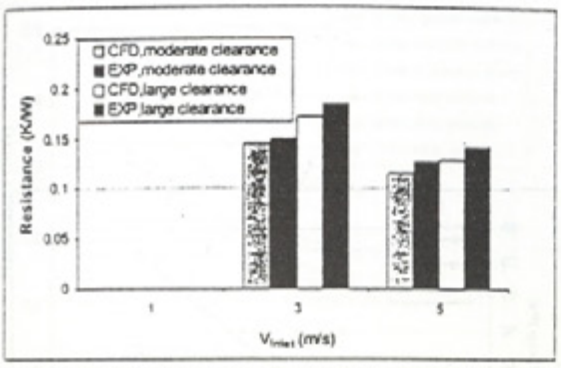

Figure 8, Partially Shrouded Heat Sink Resistance Variation with Inlet Velocity

Figures 5 - 8 serve to validate the use of a CFD tool for studying the bypass effect in high performance heat sinks. The CFD results were obtained using models of the test section to carry out simulations and will be presented in greater detail in the next section.

CFD MODELING AND ANALYSIS

Computational Fluid Dynamics (CFD) Software tools, are widely used to 'virtually' test heat sink designs and predict their thermal behavior, subject to specific design constraints. A half symmetry model using the commercially available Icepak software, developed by FLUENT Inc. [1999], was constructed to conduct parametric simulations to investigate the bypass effect. Excellent agreement (± 0.2%) was observed between the half-symmetry and full configuration cases.

Figure 9 shows a picture of the CFD model. Blocks of conductivities 220 W/mK and 150 W/mK for base and fins, respectively, were used to construct the heat sink. These thermal conducivities, specified by the manufacturer, are used to mimic the heat sink illustrated in the Figure 4(b). A zero thickness heat source, 110 × 71 mm dissipating 100W was attached to the bottom of the heat sink. The major components of the CFD test section were the no-swirl rectangular fan at one end of the duct and an opening that exhausted to atmospheric pressure at the other end. The channel length was 0.61 m, while the height and width of the channel were varied depending on the shroud configuration. The heat sink was placed 0.17 m downstream of the fan and 0.33 m upstream of the opening. The inlet ambient air temperature for this model was fixed at 25 °C.

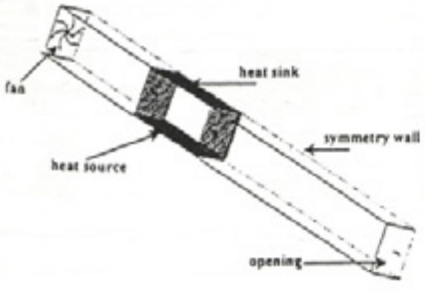

Figure 9, CFD Half Symmetry Model

For the range of air mass flow rates modeled in the CFD runs (0.004-0.036 kg/s), the Reynolds numbers inside the heat sink obtained from the analytical analysis, were found to be in the laminar domain (≤ 2800). Furthermore the CFD results determined using laminar flow were found to compare significantly better (7% error) with the experimental data than those resulting from the turbulent flow (15-20% error). The mesh size ranged between 110,000 to 210,000 elements and the solution time was in the range of 1-2 hours. The computations were carried out on IBM Winter-Hawk Nodes, Minnesota Supercomputing Institute.

The CFD results and the experimental data for the dense heat sink were found to be in good agreement, as discussed in the earlier section. Following this favorable validation, the CFD model was utilized to investigate the flow bypass effect for three different shroud configurations for the three heat sink candidate designs, as described in Table 1. The three shroud arrangements, shown in Figure 8, were constructed using a full shroud, a moderate clearance, and a large clearance, which correspond to area ratios of 1, 1.21, and 1.69, respectively. The area ratio is obtained by dividing specified duct area by the heat sink cross section area. For the partially shrouded cases b and c, the duct dimensions were extended from those in case a by factors of 1.1 and 1.3, respectively.

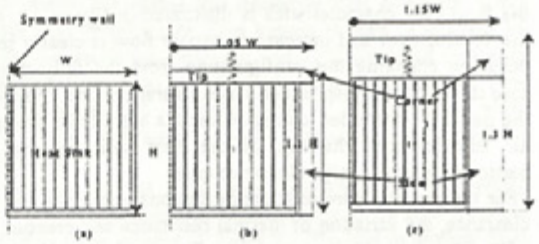

Figure 10, Ducted Heat Sink Configurations: (a) Fully Shrouded, (b) Moderate Clearance, (c) Large Clearance

Results and Discussion

Fin Density. Figure 11(a) shows the variation of thermal resistance with the mass flow rate for the three heat sink geometries in the fully shrouded configuration. R_{HS} is seen to decrease with increasing inlet velocity. As might have been anticipated, for all the mass flow rates considered, the dense heat sink, with has the greatest fin density (32 fins) has the best thermal resistance and the sparse heat sink (16 fins) is thermally the worst. Thus it can be concluded that the dense heat sink is the best geometry under the fully shrouded configuration.

The pressure drops required to achieve the thermal resistance, shown in Figure 11(a), are shown in Figure 11(b) as a function of inlet velocity for the three heat sink geometries. The parabolic dependence of pressure drop on the velocity is clearly visible for all three geometries, with the densest array experiencing a max pressure drop of 74 Pa at 5 m/s, nearly three times the pressure drop of the least dense array.

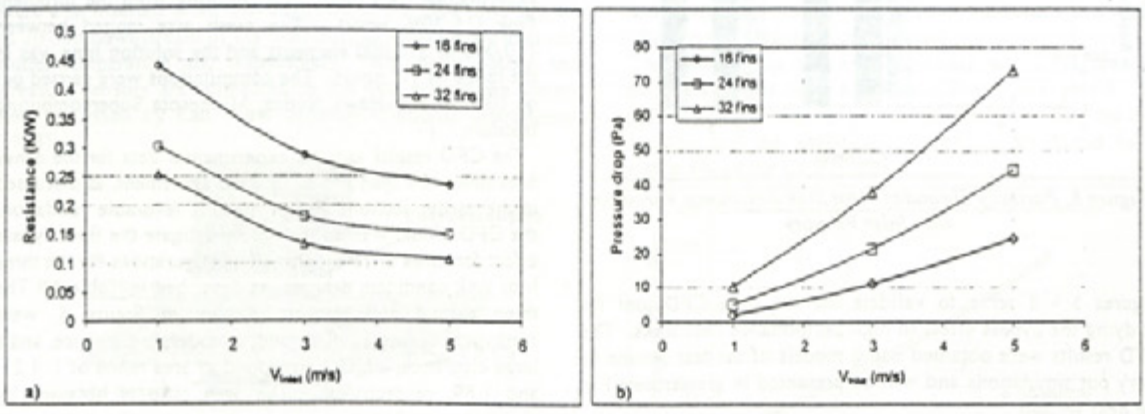

Figure 11. (a) Thermal Resistance and (b) Pressure Drop for the Fully Shrouded Configuration

Clearance. The impact of clearance around the heat sink on the fluid flow characteristics is illustrated in Figure 12, where the development and increase in bypass flow is clearly seen to occur on changing the configuration from the fully-shrouded case to the partially-shrouded large clearance case. Further, in the partially –shrouded configurations, a significant amount of air leakage from the top of the heat sink can be seen, particularly for the large clearance case.

For the partially shrouded configurations, moderate and large clearance, the variation of thermal resistance and pressure drop with the inlet velocity is seen in Figure 13. For the higher velocities of 3-5 m/s, the thermohydraulic heat sink behavior shows the geometries with higher fin densities to be thermally superior. However for the large clearance case with lower velocities (<3 m/s), the thermal resistance for the moderate heat sink is superior to that of dense heat sink, indicating the detrimental effects of flow bypass on very dense heat sinks.

Comparing the results for the extreme configurations such as fully-shrouded and large clearance case, for an inlet velocity of 1 m/s, the resistance for sparse, moderate and dense heat sinks, are found to diminish by 8%, 31%, and 74%, respectively. For V_{inlet} = 5 m/s the thermal resistance dropped by 6%, 10%, 19%, respectively. Thus the thermal resistance for each of the three geometries is found to follow an asymptotic behavior with increasing inlet duct velocity. For the heat sink volume used in this study, the deleterious effects of flow bypass are seen to have a larger influence for inlet velocities lower than 3 m/s and shroud clearances greater than 10%. It is to be noted that, for the large clearance configuration and low air velocities, moderately dense heat sink is estimated to be the most favored geometry. As explained in the case of full-shroud configuration, the parabolic dependence of pressure drop on the velocity is also seen here for all three geometries. However, in the cases of the densest array at 5 m/s, the pressure drop decreases from 74 Pa to 52 Pa for the large clearance configuration. For all fin densities, characterized in this study, going from fully-shrouded to large clearance configuration resulted in approximately 50 % decrease of the pressure drop.

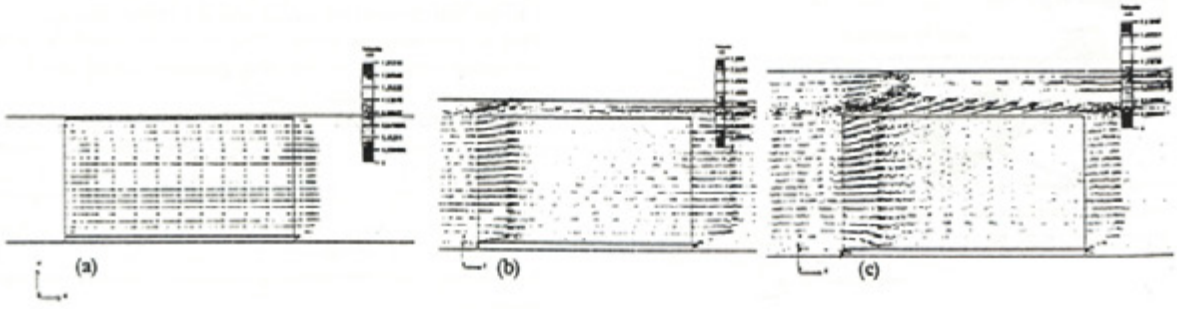

Figure 12. Flow Bypass, Moderate Heat Sink, (a) Fully-Shrouded (b) Moderate Clearance, (c) Large Clearance

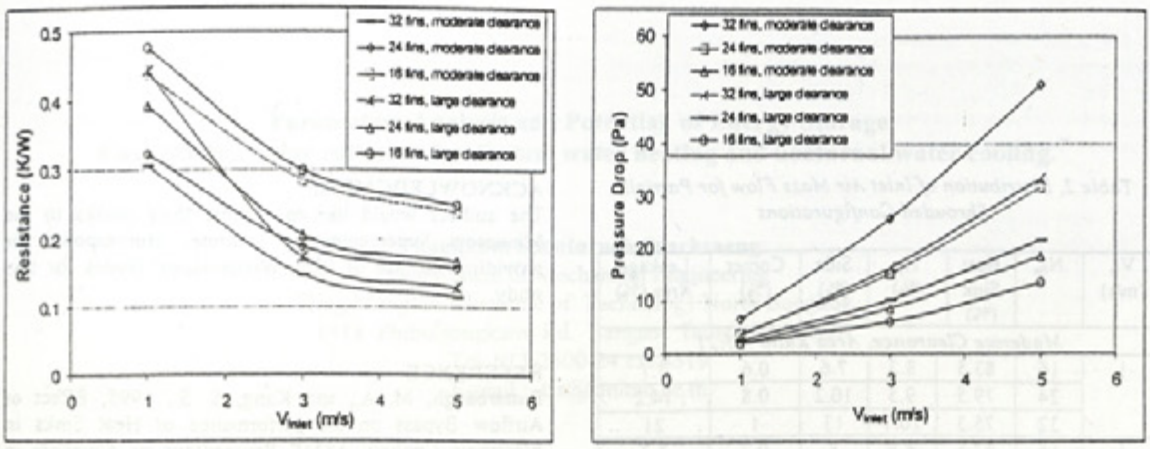

Figure 13. Effect of Clearance on Heat Sink Resistance and Pressure Drop

Minimum Resistance. A detailed parametric CFD analysis, the results of which are shown in Figure 14 was performed to determine the optimum fin density for the operating conditions of inlet velocity 1 m/s and various clearance ratios. Interestingly, it was found that for a specific heat sink volume with a fixed inlet duct velocity and a given bypass clearance, there exists an optimum heat sink geometry that will minimize the thermal resistance and maximize array heat transfer. This trend is consistent with the findings of Wirtz et al [1994]. The optimum fin density was found to be 24 and 32 fin for large and moderate clearance configurations, respectively. For the moderate clearance configuration, for the range of N_{fin} between 26 and 36, the thermal resistance is found to be relatively insensitive to the fin number. Thus increasing surface area by adding fins, would result in increased mass and cost, without significant improvement in the thermal resistance. On the other hand, for the fully shrouded case, increasing fin density continues to improve performance.

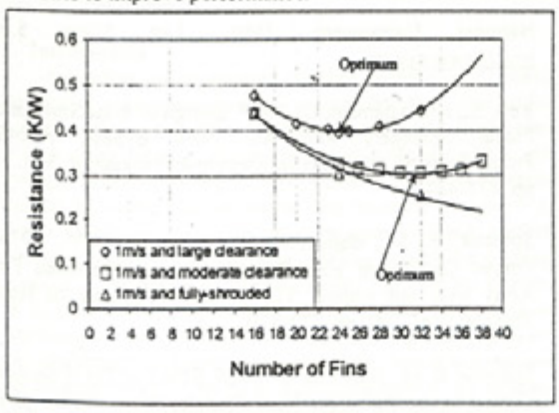

Figure 14. Variation of Heat Sink Resistance with Fin Density

Bypass Ratio. Table 2 provides data regarding the distribution of air flow through the various regions for the duct, i.e. the heat sink, the side clearance, the tip clearance, the duct corner, and also directly from the top of heat sink (leakage area). The flow bypass is seen to increase with increasing fin density. For the same inlet air velocity and shroud clearance, the dense heat sink experiences flow bypass greater than sparse and moderate heat sinks. Comparing the results for sparse and moderate heat sinks for 1 m/s inlet duct velocity, the flow bypass is seen to increase by 10% for moderate clearance and 22% for large clearance configuration. For the moderate clearance case, the flow bypass appears to be independent of inlet velocity, while for larger clearance a small reduction in bypass is observed.

The flow leakage from the top of the heat sink will reduce its effectiveness and this phenomena may be seen from the extreme right column in Table 2. The loss of airflow from the top is found to reduce with inlet air velocity, for a given heat sink and shroud configuration, and is seen to increase with bypass clearance for a fixed velocity. It is also interesting to note that this air leakage occurs to a greater extent for array geometries with higher fin densities. Further, comparing the flow distribution at the tip and sides, due to their area ratio of 1, it can be seen that approximately the same percentage of air is going trough these areas. Therefore, the flow doesn't have preferable path and it is equally distributed in these two areas.

Thus, an observation for the flow distribution through the duct, appears to suggest that increases in inlet velocity lead to dominance of the inertial component of the flow, even though the fluid resistance is higher in the finned area. Hence, very little increases in the flow bypass are seen from increases in the inlet velocity. With respect to the air leakage from the top of the heat sink, a modification to the fin array by addition of a top plate may improve the heat sink design.

Table 2. Distribution of Inlet Air Mass Flow for Partially Shrouded Configurations

V_{in} (m/s)	N_{fin}	Heat Sink (%)	Tip (%)	Side (%)	Corner (%)	Leakage Area (%)
Moderate Clearance, Area Ratio = 1.21						
1	16	83.5	8.3	7.6	0.6	7.7
	24	79.5	9.5	10.2	0.8	14.2
	32	75.3	10.7	13	1	21
3	16	82.5	8.8	8	0.7	5.3
	24	80	9.6	9.6	0.8	9.1
	32	77.4	10.3	11.3	1	13.3
5	16	82	9	8.2	0.8	4.3
	24	79.9	9.6	9.6	0.9	7.2
	32	77.9	10.2	10.9	1	10.6
Large Clearance, Area Ratio = 1.69						
1	16	52.9	20.3	21.1	5.7	12.7
	24	47.1	21.8	24.5	6.6	19.5
	32	41.1	23.8	28	7.5	24.3
3	16	53.9	19.9	20.3	5.9	7.7
	24	50.3	20.9	22.4	6.4	12.1
	32	46.6	21.9	24.6	6.9	17.2
5	16	54.2	19.7	20.2	5.9	6.1
	24	51.3	20.6	21.8	6.3	9.7
	32	48.2	21.5	23.6	6.7	13.9

CFD simulations were also performed using three different mass flow rates for the three candidate heat sinks, for the three varying shroud configurations, yielding trends consistent with the constant inlet velocity runs seen in Figures 11 and 13 as well as the data in Table 2.

CONCLUSION

CFD studies were carried out to investigate the effect of fin density, inlet duct velocity, and clearance on the extent of flow bypass and thermal performance of the heat sink. For validation purposes specific CFD results were shown to have good comparison with experimental data and analytical predictions. The flow bypass is seen to increase with increasing fin density and clearance, and is found to be relatively insensitive to inlet duct velocity. For the heat sink volume characterized in this study, the deleterious effects of flow bypass are seen to have a larger influence for low inlet velocities and large shroud clearances. The loss of airflow from the top of the heat sink is found to decrease with inlet air velocity, for an array geometry and shroud configuration, and is seen to increase with bypass clearance for a fixed velocity. It is also interesting to note that this air leakage occurs to a greater extent for array geometries with higher fin densities. An optimum geometry, for a fixed inlet duct velocity, bypass clearance, fixed heat sink volume, and constant thickness, was determined.

ACKNOWLEDGMENT

The authors would like to express their thanks to the Minnesota Supercomputing Institute, Minneapolis, for providing the use of IBM Winter-Hawk Nodes for this study.

REFERENCE

Butterbaugh, M. A., and Kang, S. S., 1995, Effect of Airflow Bypass on the performance of Heat Sinks in Electronic Cooling, ASME Proceedings of Advances in Electronic Packaging, Vol. 2, pp. 843-848.

FLUENT Inc., 1999, IcePak Reference Manual 3.0., http://www.fluent.com/icepak

Holahan, M.F., Kang, S.S., Bar-Cohen, A., 1996, A Flowstream Based Analytical Model for Design of Parallel Plate Heatsinks, 1996 ASME HTD-Vol. 329 Volume 7, National Heat Transfer Conference- Vol 7. pp. 63-71.

Iwasaki, H., Sasaki, T., Ishizuka, M., 1994, Cooling Performance for Plate Fins for Multichip Modules, Proceedings of the Intersociety Conference on Thermal Phenomena, pp. 144-147.

Kakac, S., Shah, R. K., Aung, W., 1987, Handbook of Single-Phase Convective Heat Transfer, Second Edition, pp. 3-35, 3-42, Wiley & Sons, New York.

Kays, W. M., and London, A. L., 1984, Compact Heat Exchangers, Third Edition., pp. 108-112, McGraw Hill, Inc., New-York

National Instruments, 1998, Lab View 5.0, http://www.ni.com

Reis, E., and Altemani, C., 1999, Design of Heat Sinks and Planar Spreaders with Air Flow Bypass, ASME Proceedings of Advances in Electronic Packaging, Vol. 1, pp. 477-484.

Sparrow, E. M., Baliga, B. R., Patankar, S. V., 1978, Forced Convection Heat Transfer from a Shrouded Fin Array with and without Tip Clearance, Journal of Heat Transfer, Vol. 100, pp. 572-579.

Sparrow, E. M., Kadle, D. S., 1986, Effect of Tip to Shroud Clearance on Turbulent Heat Transfer from a Shrouded, Longitudinal Fin Array, Journal of Heat Transfer, Vol. 108, pp. 519-524.

Wirtz, R. A., Chen, W., Zhou, R., 1994, Effect of Flow Bypass on the Performance of Longitudinal Fin Heat Sinks, ASME Journal of Electronic Packaging, vol.116, pp.206-211.